



Cite this: *RSC Sustainability*, 2025, **3**, 1788

General component additivity, reaction engineering, and machine learning models for hydrothermal liquefaction[†]

Peter M. Guirguis  and Phillip E. Savage  *

Hydrothermal liquefaction (HTL) is the process of breaking down renewable biomass resources in hot compressed water to produce crude bio-oil. There are more than a thousand experimental biocrude yields in the literature. We use this extensive data set to parameterize new models for HTL. These new models are general in that they can handle any biomass feedstock and HTL at any set of reaction conditions. We report new component additivity, reaction engineering, and machine learning models that correlate the experimental data and predict biocrude yields with a median absolute residual of no more than 6.3 wt%. These new models predict literature biocrude yields more accurately than any of the previously published models for HTL of biomass. The new component additivity model employs coefficients that are continuous functions of reaction severity and biomass loading (wt%). The new reaction engineering model includes the possibility of portions of the initial feedstock (e.g., lipids) being in one of the product fractions (e.g., biocrude) at $t = 0$. The decision tree model provided the best fit of the biocrude yields, but it also had far more parameters than did the other models. The component additivity model was superior to the reaction engineering model in fitting the HTL biocrude yields. However, the reaction engineering model is statistically better than the component additivity model at predicting biocrude yields. We use the new models to identify HTL reaction conditions that would maximize yields of biocrude for different types of biomass yet to be investigated experimentally.

Received 22nd November 2024
Accepted 17th February 2025

DOI: 10.1039/d4su00737a
rsc.li/rscsus

Sustainability spotlight

Hydrothermal liquefaction (HTL) provides a sustainable route to convert wet biomass into renewable biocrude oil, addressing the global need for cleaner energy. This work advances sustainability by creating predictive models that optimize HTL efficiency across varied feedstocks, reducing resource waste and enhancing biofuel viability. By leveraging a large dataset and innovative modeling approaches, this study supports UN SDGs 7 (Affordable and Clean Energy) and 12 (Responsible Consumption and Production), offering tools for better process design, economic assessments, and environmental impact reduction in biofuel production.

1 Introduction

Hydrothermal liquefaction (HTL) converts renewable wet biomass into biocrude oil *via* thermochemical processing around 150–600 °C, 30 seconds to 1.5 hours, and 10–25 MPa. A wide variety of biomasses have been used as feedstocks in HTL. These include micro and macro-algae, food waste, sludge, and lignocellulosic biomass. There has been work examining the technoeconomic feasibility of HTL, the life-cycle environmental impacts, and operation of continuous processes approaching commercial scale.^{1–7} Accurate mathematical models that connect the HTL process variables (e.g., temperature, time) and

feedstock composition with important HTL outputs (e.g., yield and quality of biocrude oil) would facilitate more complete economic and environmental assessments as well as better-optimized process designs.

Modeling has been an active area in HTL research, and one of three approaches is generally taken. One approach is to assume some output from HTL (e.g., biocrude yield) can be estimated as the sum of the individual contributions from different biochemical components in biomass. A second approach is to assume that the numerous components and individual elementary reactions taking place during HTL can be described by global reaction pathways that connect lumped reaction products (e.g., biocrude, aqueous-phase products, solids, gases). Standard chemical reaction engineering procedures then lead to mathematical models. The final approach is to use machine learning to fit a set of experimental data.

Chemical Engineering Department, Pennsylvania State University, 121D CBEB Building, University Park, PA 16802, USA. E-mail: psavage@psu.edu

† Electronic supplementary information (ESI) available. See DOI: <https://doi.org/10.1039/d4su00737a>



The models published to date have been handicapped by using only a small set of data for parameter estimation. In a typical investigation, the researchers would conduct HTL experiments with some specific biomass, formulate a model, and then use their results to determine the model parameters. This approach works well if interest is limited solely to that specific biomass, but the model lacks more general applicability. Moreover, the field has progressed and there is now a wealth of published data on HTL outputs from a large range of biomass feedstocks over a wide range of processing conditions.

In our previous work, we used a dataset with 1294 unique experimental biocrude yields (3867 data points in total, for yields of solid, biocrude, aqueous, and gas-phase products) to review and assess all the published component additivity models and reaction engineering models in the literature. We used the fitted parameters provided in each publication and calculated the biocrude yields each model would predict.⁸ Some models worked well for some feedstocks, but none could give accurate predictions of biocrude yield for all biomass feedstocks at all HTL operating conditions. Yet, it is precisely this type of robust, general model, that would be most useful in the field. In the present work, we use the new, large dataset that is now available to develop the most general component additivity, reaction engineering, and machine-learning models to date for predicting biocrude yields from HTL of biomass. These models can predict biocrude yields for HTL of any biomass feedstock at any combination of processing time and temperature.

2 Data and methods

We used 1144 unique measurements of the biocrude yield from HTL along with 2130 corresponding measurements for the yields of solid, aqueous, and gas phase product fractions from HTL.⁸ We were unable to use 150 of the biocrude yields in the database as they were not accompanied by the biomass loading or compositional information. The feedstocks in the dataset include whole biomass such as wood, algae, food waste, and sewage sludge; defatted biomass; isolated biomass components such as protein isolate, and kraft alkaline and dealkaline lignin, as well as model biomolecules such as stearic acid. For each reported HTL product yield, we collected the set-point temperature of the heating source, the holding and heating times of the reactor, the biomass loading (mass percentage of feedstock to water), and the reactor heating rate, if available.

We use 90% of the dataset for model discrimination and parameter estimation and 10% of the dataset for testing predictive ability. The 10% subset was chosen by first using a pseudo-random algorithm, which selects one data point randomly from each publication with more than two biocrude yields reported. The remainder of the 10% was filled randomly.

We use seven different statistical metrics to evaluate the fit and predictive ability of a given model. We use the median residual, $\text{Med}[\varepsilon]$, in eqn (1), the mean absolute residual, $\overline{|\varepsilon|}$, in eqn (2), median absolute residual, $\text{Med}[|\varepsilon|]$, in eqn (3) Mean Absolute Percent Error (MAPE) in eqn (4), Akaike Information Criteria (AIC) for normally distributed error in eqn (5), and the

percentage of predictions within 5 wt% and 10 wt% of the experimental values.

$$\text{Med}[\varepsilon] = \begin{cases} \varepsilon \left[\frac{n+1}{2} \right] & \text{if } n \text{ is odd} \\ \frac{\varepsilon \left[\frac{n}{2} \right] + \varepsilon \left[\frac{n}{2} + 1 \right]}{2} & \text{if } n \text{ is even} \end{cases} \quad (1)$$

$$\overline{|\varepsilon|} = \frac{\sum |y_{\text{calc}} - y_{\text{exp}}|}{n} \quad (2)$$

$$\text{Med}[|\varepsilon|] = \begin{cases} \left| \varepsilon \left[\frac{n+1}{2} \right] \right| & \text{if } n \text{ is odd} \\ \frac{\left| \varepsilon \left[\frac{n}{2} \right] \right| + \left| \varepsilon \left[\frac{n}{2} + 1 \right] \right|}{2} & \text{if } n \text{ is even} \end{cases} \quad (3)$$

$$\text{MAPE} = \frac{100\%}{n} \sum \left| \frac{y_{\text{calc}} - y_{\text{exp}}}{y_{\text{exp}}} \right| \text{ where } y_{\text{exp}} \neq 0 \quad (4)$$

$$\text{AIC} = 2k + n \ln \left(\frac{\sum (y_{\text{calc}} - y_{\text{exp}})^2}{n} \right) \quad (5)$$

where ε is the residual, n is the number of data points, y_{calc} is the value calculated by the model, y_{exp} is the experimental value, and k is the number of parameters fitted.

The $\text{Med}[\varepsilon]$ statistic reveals any bias in the parameter estimation. An unbiased $\text{Med}[\varepsilon]$ is zero, meaning the same number of residuals are below zero as are above zero. The values for $\overline{|\varepsilon|}$, $\text{Med}[|\varepsilon|]$ and MAPE demonstrate how close the model predictions are to the experimental data. AIC is a relative measure of goodness of fit leveraging the likelihood function while avoiding over-fitting the model by penalizing use of an unnecessarily large number of fitted parameters. A low AIC indicates that the error is randomly distributed based on a normal distribution weighed against the number of parameters. The AIC metric is a relative score to compare models. The score is only meaningful if the parameters are the optimal (fitted) parameters for the data used.

3 Component additivity model

A component additivity model is an algebraic expression as in eqn (6) that uses the composition of a biomass feedstock to predict some outcome from HTL. These outcomes typically focus on the biocrude and have included its heating value, elemental composition, and yield Y_B .

$$\begin{aligned} Y_B \% = & \sum_{i=1}^{11} C_i X_i \\ & + \sum_{j=1}^4 \sum_{k=j+1}^4 C_{j,k} X_j X_k \\ & + \sum_{j=1}^4 \sum_{k=j+1}^4 \sum_{l=k+1}^4 C_{j,k,l} X_j X_k X_l + C_{j,k,l,m} X_j X_k X_l X_m \end{aligned} \quad (6)$$

X_i is the mass fraction of biochemical component i in the biomass feedstock, and the subscripted C 's are fitted



parameters. The present general model considers 11 individual biomass components. They are cellulose (Ce), hemicellulose (He), starch (St), other uncharacterized carbohydrates (Un), polypeptides (Pe), lipids (Lp), lignin (Lg), saccharides (Sa), amino acids (AA), fatty acids (FA), and phenolics (Ph). There are four lumped biomass components, total carbohydrates (C_t), total proteins (P_t), total fats (F_t), and total lignin (L_t). C_t collects together cellulose, hemicellulose, starch, other uncharacterized carbohydrates, and saccharides. P_t collects polypeptides and amino acids. F_t collects lipids and fatty acids. L_t collects lignin and phenolics.

Initial component additivity models for HTL considered just a single time and temperature combination and their predictions were limited to HTL conditions near that single combination. Subsequent component additivity models incorporated the effects of temperature and time, often by using different discrete sets of parameters for different HTL times and temperatures.^{9–12} A general model for HTL needs to account for the influences of reaction time and temperature, ideally as a continuous function. Herein we use the severity index (SI) (eqn (7)) to combine the effects of time and temperature into a single variable.

$$SI = \int_0^{t_f} e^{-\frac{E_a}{R} \left(\frac{1}{T(t)} - \frac{1}{T_0} \right)} dt \quad (7)$$

where t_f is the reaction time in minutes, T is the absolute temperature of the heat source, E_a is an activation energy (taken as 83 kJ mol⁻¹), T_0 is a reference temperature (taken as 700 K),¹³ and R is the gas constant (8.314 J mol⁻¹ K⁻¹).

When the reactor heating profile was provided in the publication, we modeled the reactor temperature as a function of

time using a Morse-like potential shown in eqn (8). Otherwise, the reaction is treated as isothermal.

$$T(t) = T_f \left(1 - e^{-bt + \ln[1 - \sqrt{25/T_f}]} \right)^2 \quad (8)$$

T_f is the temperature of the heat source, and b is a fitted constant. Finally, we use differences between two sigmoidal functions, g , eqn (9), one increasing and one decreasing, to create parameters that vary continuously with reaction severity and biomass loading as shown in eqn (10).

$$g(x, k, s) = \frac{1}{1 + e^{-k(x-s)}} \quad (9)$$

$$C(\ln(SI), w) = L(g(\ln(SI), k_1, s_1) - g(\ln(SI), k_2, s_2) + M) \quad (10)$$

$$(g(w, k_3, s_3) - g(w, k_4, s_4))$$

where w is the biomass loading in wt% (mass solids/mass water%) and L , k_1 , k_2 , k_3 , k_4 , s_1 , s_2 , s_3 , s_4 , and M are fitted parameters. The value of the sigmoidal function varies only between 0 and 1, so the fitted parameter L represents the highest (or lowest if negative) value the function can reach. M is the limit as $\ln(SI)$ goes to negative and positive infinity.

We fit the models using *Python version 3.11.7, 64-bit*. We used the *minimize* function from the *scipy.optimize version 1.13.0* library with the Nelder–Mead method to minimize the sum of absolute residuals in eqn (2).¹⁴ The component additivity model that best fits and predicts the collected data for biocrude yields from HTL of biomass is shown in eqn (11). The C parameters are functions of the severity index and the biomass loading (wt%), per eqn (9). Numerical values for the C parameters for this model at different values of SI and different biomass loadings are provided in Table S1.† There are 15 C parameters

Table 1 Parameters evaluated for the component additivity model in eqn (11)

Parameters	Parameters evaluated at different $\ln(SI)$ and fixed 10 (g _{solids} /g _{water})% loading							Parameters evaluated at different loadings (g _{solids} /g _{water}) % and fixed $\ln(SI) = 1.64$ which corresponds to 350 °C and 30 min						
	-10	-5	-2.5	0	2.5	5	10	1.64	1.64	1.64	1.64	1.64	1.64	1.64
ln(SI)														
Loading mass	10	10	10	10	10	10	10	2.5	5	10	15	20	25	30
C_{St}	1.82	1.81	2.17	7.18	8.34	8.35	8.33	26.7	18.9	8.28	3.24	1.21	0.444	0.162
C_{Ce}	2.57	1.44	4.18	10.0	12.0	11.3	8.96	16.0	14.7	11.8	9.06	6.60	4.61	3.12
C_{He}	8.20	7.99	6.85	26.8	28.5	11.2	8.24	55.1	51.9	38.5	25.0	14.7	8.07	4.25
C_{Pe}	16.0	16.0	16.0	16.0	18.5	18.5	18.5	4.47×10^{-7}	0.000185	18.5	44.9	44.9	44.9	44.9
C_{Lp}	63.3	70.5	75.5	80.5	78.9	49.0	30.3	61.4	69.3	81.4	88.5	91.4	90.1	83.3
C_{Lg}	0.894	0.894	0.894	2.35	14.9	0.894	0.894	0.0692	5.46	14.7	20.6	23.7	25.1	25.7
C_{Sa}	1.19×10^{-5}	2.49×10^{-5}	1.57	1.57	0.930	1.19×10^{-5}	1.19×10^{-5}	0.515	0.884	1.57	2.15	2.62	2.98	3.25
C_{AA}	1.02	1.02	1.02	1.05	1.33	3.61	0.258	0.237	0.554	1.16	1.72	2.19	2.58	2.89
C_{FA}	36.3	49.6	55.6	60.3	15.9	15.0	17.2	0.0160	64.3	62.6	60.9	59.3	57.6	56.0
C_{Ph}	28.8	41.1	47.1	47.1	26.3	3.88	2.98	0.0584	29.0	36.1	36.2	36.2	36.2	36.2
$C_{C_{t,P_t}}$	-27.1	-10.1	10.2	39.8	37.8	-62.9	-40.4	46.7	49.3	54.4	59.3	-27.9	-23.7	-19.9
$C_{C_{t,F_t}}$	13.8	27.0	33.3	-22.8	-18.6	-15.3	-11.3	-5.93	-52.4	-20.0	-6.23	-1.81	-0.516	-0.146
$C_{P_{t,F_t}}$	-92.2	-92.2	-92.2	-92.2	-92.2	-92.2	91.8	86.7	90.3	-92.2	-86.4	-79.3	-72.5	-65.9
$C_{C_{t,P_t,F_t}}$	-366	-137	65.7	308	542	727	925	268	344	466	-38.6	-13.6	-4.65	-1.57
C_{C_{t,P_t},L_t}	125	248	225	180	132	90.0	36.7	-155	-151	148	131	115	99.7	85.7



and 150 parameters in total. Table 1 gives the parameters evaluated at different values of $\ln(\text{SI})$ at 10% loading mass and different loading masses at $\ln(\text{SI}) = 1.64$.

$$Y_B\% = \sum_{i=1}^{10} C_i X_i + \sum_{j=1}^3 \sum_{k=j+1}^3 C_{j,k} X_j X_k + C_{C_t, P_t, F_t} X_{C_t} X_{P_t} X_{F_t} + C_{C_t, F_t, L_t} X_{C_t} X_{F_t} X_{L_t} \quad (11)$$

This model is a simpler version of the more general model in eqn (6). Analysis of that more general model revealed that many interaction terms were statistically insignificant and could be omitted. More specifically, we were able to combine cellulose and the uncategorized carbohydrates into a single biomass pseudo-component. This consolidation reduced the number of individual biomass components to 10 (from 11). We also determined that many interactions involving total lignin were statistically insignificant. Binary interactions are only between C_t , P_t , and F_t .

The values of C_i represent the expected yield of biocrude from HTL of that component alone at the given conditions. For the three carbohydrates, note that C_i decreases as the biomass loading increases. This trend aligns with and is influenced by the data from Gollakota and Savage,¹⁵ which showed the biocrude yield decreasing with increasing biomass loading for HTL of polysaccharides. For nearly all of the individual biomass components, the biocrude yield (C_i) first increases and then decreases with increasing reaction severity.

Fig. 1 compares the calculated and experimental biocrude yields for the data set used to fit and predictions for the model parameters. Table 2 summarizes the statistics for each. The model predicts biocrude yields to within 6.3 wt% median absolute error.

Fig. 2 compares predictions from the new component additivity model with predictions from 17 component additivity models^{9–12,16–25} in the literature, using the parameters provided in literature. We tested five models capable of predicting

Table 2 Statistical analysis for fitting and prediction for the new component additivity model

Statistic	Fit	Prediction
Number of data points	1032	112
Med[ε]	0.0233	1.61
$ \varepsilon $	6.18	8.33
Med[$ \varepsilon $]	4.07	6.33
MAPE	75.5	67.9
AIC (wt%)	4812.9	—
% < 5	56.7	42.9
% < 10	78.8	67.0

biocrude yields from HTL of lignin-containing biomass, shown in Fig. 2a, and 12 models that did not include lignin as part of the composition, shown in Fig. 2b. The models without lignin were tested on the subset of the prediction dataset that contained no lignin-containing biomass. Statistical details are available in Tables S2 and S3† in the ESI.† The new model provides the best predictions, both statistically and visually, compared to the published component additivity models.

In addition to comparing the new model to the published models with the published parameters, we fitted the general forms of these published models to the large datasets to get updated parameter values. Even here, the predictions from the new model were superior to those from the published models.

4 Reaction engineering model

Reaction engineering models are based on chemical reaction networks that describe the conversion of material from one chemical component to another (e.g., from biomass to biocrude). Combining reaction rate equations for each path in the network with the design equation for the type of chemical reactor used in the HTL experiments leads to a set of simultaneous equations that govern the evolution of species concentrations over time. All the biocrude yields in the database used herein were obtained in batch reactors, and we used the appropriate set of differential equations for the modeling. We used mass action rate equations and Arrhenius rate constants. The Arrhenius parameters served as the fitted parameters.

A general reaction engineering model for HTL of biomass would include all the biopolymers likely to be in biomass as reactants, allow each to react at its own rate, and account for interactions between biochemical components that influence the yields of product fractions. A general model would also be able to handle smaller biomolecules such as amino acids, saccharides, phenolics, and fatty acids, that are not in polymeric form. The model developed herein meets these criteria. Biomass is treated as a mixture of protein, lipids, lignin, and carbohydrates. The final group is subdivided into cellulose, hemicellulose, and starch, to account for reactivity differences for these polysaccharides. Carbohydrates that are not clearly identified as one of these three in the published work are treated as cellulose for modeling purposes. The reaction network (Fig. 3) allows for binary interactions between carbohydrates, proteins, lipids, and lignin in the biomass as they

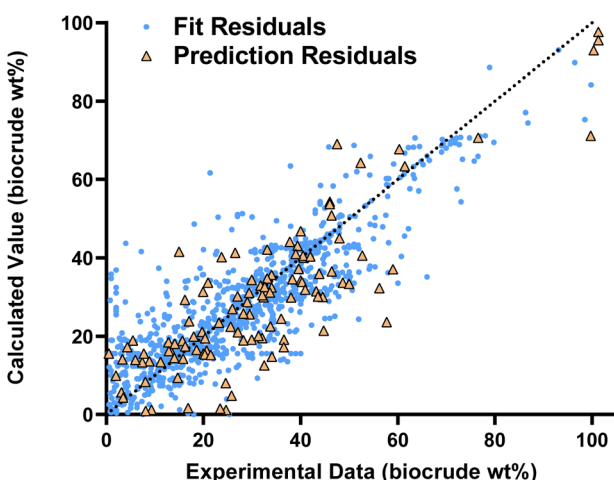


Fig. 1 Parity plot for the new component additivity model fit and predictions.

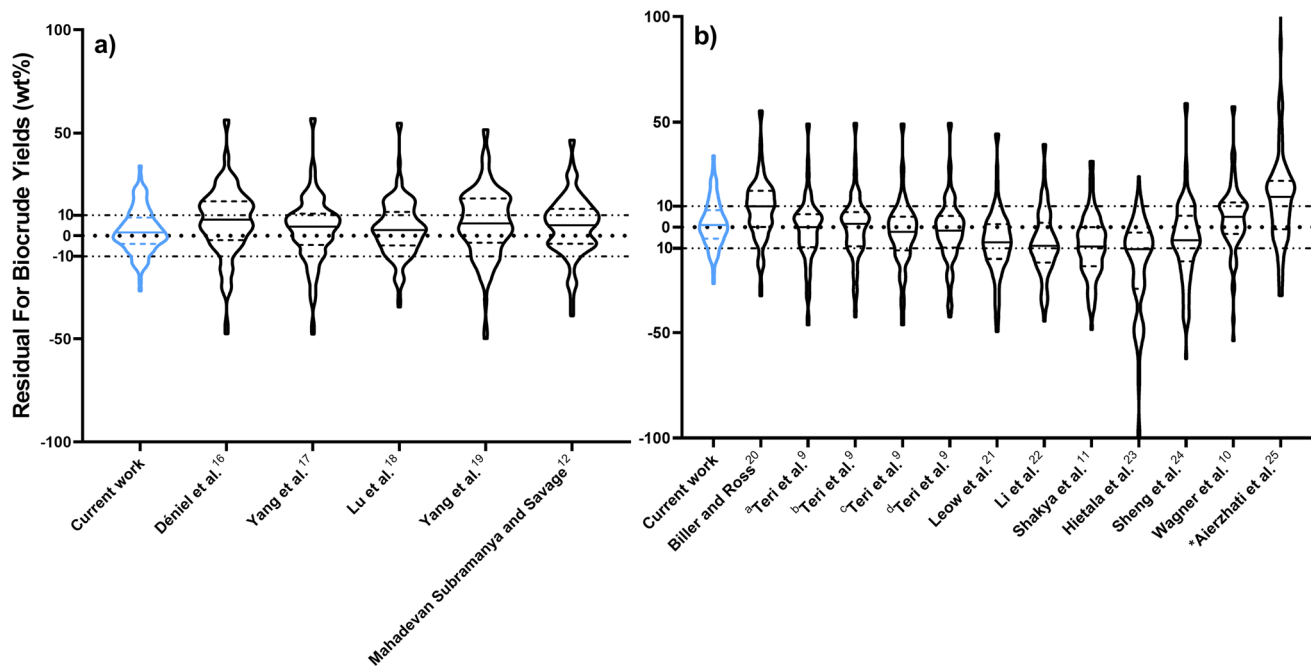


Fig. 2 Comparing predictions from component additivity models using a violin plot. The outer curve is the distribution of the residuals, the solid line in the middle is the median residual, and the dashed lines are the upper and lower quartiles: (a) Models that include lignin-containing biomass. (b) Models without lignin. ^a The component additivity model using HTL of soy protein, cornstarch, and castor oil. ^b The component additivity model using HTL of cellulose, albumin, and sunflower oil. ^c The component additivity model in ^a with interactions. ^d is the component additivity model in ^b with interactions. *The residuals extends 167 wt%.

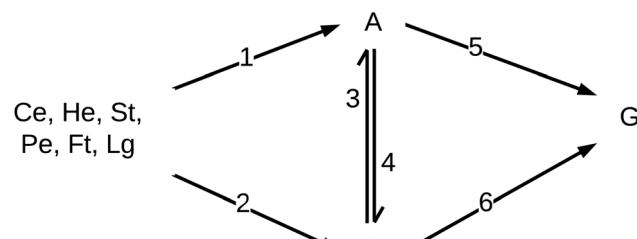


Fig. 3 Reaction network for modeling HTL of biomass.

react to form aqueous-phase (A) and biocrude (B) products. Products in the aqueous phase can react to form gases (G) or molecules that partition into the biocrude phase. Likewise, molecules in the biocrude phase can react to form a water-soluble product or a gaseous product.

Eqn (12) provides the governing differential equations.

$$\begin{aligned}
 \frac{dX_i}{dt} &= -(k_{1,i} + k_{2,i})X_i - \sum_r^2 \sum_j^4 k_{r,ij}X_iX_j \\
 \frac{dX_A}{dt} &= \sum_i^6 k_{1,i}X_i + 2 \sum_m^4 \sum_{n=m+1}^4 k_{1,m,n}X_mX_n - (k_3 + k_5)X_A + k_4X_B \\
 \frac{dX_B}{dt} &= \sum_i^6 k_{2,i}X_i + 2 \sum_m^4 \sum_{n=m+1}^4 k_{2,m,n}X_mX_n - (k_4 + k_6)X_B + k_3X_A \\
 \frac{dX_G}{dt} &= k_5X_A + k_6X_B
 \end{aligned} \tag{12}$$

X denotes mass fraction, *k* denotes a rate constant, *i* denote one of the biopolymers or lipids, *j*, *m*, and *n* correspond to biochemical components that have binary interactions, and *r* is the reaction path for biomass conversion (1 or 2), where *i* ≠ *j* and *i* ⊈ *j*.

The HTL products are defined operationally as being gases, solids, or material soluble in water or in an organic solvent (biocrude). In many instances, material present in the original, unreacted biomass can be extracted by water or an organic solvent. Accordingly, these systems would contain “biocrude” molecules and “aqueous-phase product” molecules, even before HTL takes place. The initial conditions for the present model accounts for these materials being extractable into those phases at *t* = 0, before the HTL reaction has begun. We take all lipids and fatty acids to be in the biocrude phase at *t* = 0. We also take 60 wt% of any phenolics present and 30% of any amino acids initially present in the feedstock to be in the biocrude phase.²⁶ The balance of these smaller biomolecules would reside in the aqueous phase, along with any saccharides initially present in the biomass feedstock. We take 46 wt% of the protein, 3 wt% of the hemicellulose, and 11 wt% of the starch to be in the aqueous phase at *t* = 0.²⁷ The rest of the biopolymers in the biomass feedstock are taken to reside in the solid phase when HTL begins. Through the use of the reaction network for the biopolymers and product fractions and these initial conditions for any smaller biomolecules, we have developed a general model that can be applied to a wide range of biomass feedstocks. We assume the interactions of the other biopolymers with the polysaccharides (Ps), cellulose, hemicellulose and

Table 3 Parameters for the reaction engineering model in Fig. 3 coupled with eqn (12)

Parameter label	$\ln[A]$ ($\ln[\text{min}^{-1}]$)	E_a (kJ mol $^{-1}$)	k @350 °C (min $^{-1}$)	Parameter label	$\ln[A]$ ($\ln[\text{min}^{-1}]$)	E_a (kJ mol $^{-1}$)	k @350 °C (min $^{-1}$)
$k_{1,\text{Pe}}$	-0.107	0.00860	0.897	k_{1,Pe,F_t}	40.6	203	4.26
k_{1,F_t}	10.2	33.5	40.7	$k_{1,\text{Pe},\text{Ps}}$	10.9	105	9.04×10^{-5}
$k_{1,\text{Ce}}$	7.55	47.9	0.184	$k_{1,\text{Pe},\text{Lg}}$	20.6	85.5	62.7
$k_{1,\text{He}}$	13.8	88.1	0.0387	$k_{1,\text{F}_i,\text{Ps}}$	7.88	25.2	20.2
k_{1,S_t}	7.42	40.5	0.668	$k_{1,\text{F}_i,\text{Lg}}$	4.73	1.33	87.6
$k_{1,\text{Lg}}$	-2.82	4.35	0.0257	$k_{1,\text{Ps},\text{Lg}}$	45.3	248	0.0758
$k_{2,\text{Pe}}$	0.370	5.18	0.533	k_{2,Pe,F_t}	15.4	54.5	126
k_{2,F_t}	1.73	3.39	2.93	$k_{2,\text{Pe},\text{Ps}}$	9.62	49.7	1.02
$k_{2,\text{Ce}}$	10.1	69.9	0.0353	$k_{2,\text{Pe},\text{Lg}}$	4.47	17.9	2.74
$k_{2,\text{He}}$	14.3	86.8	0.0887	$k_{2,\text{F}_i,\text{Ps}}$	16.0	57.4	133
k_{2,S_t}	9.18	58.7	0.116	$k_{2,\text{F}_i,\text{Lg}}$	19.1	36.7	1.66×10^5
$k_{2,\text{Lg}}$	-2.05	13.9	0.00872	$k_{2,\text{Ps},\text{Lg}}$	25.7	227	1.35×10^{-8}
k_3	6.30	214	6.07×10^{-16}	k_5	-2.86	10.9	0.00696
k_4	2.11	48.9	0.00066	k_6	14.3	107	0.00181

starch, is identical. Fitting the model to the large dataset gives the parameter values in Table 3. The model has 56 parameters.

We fit all the models in *Python version 3.11.7, 64-bit* using *solve_ivp* from *scipy.integrate version 1.13.0* with the *Radau* stiff solver to calculate the numerical solution for the system of ODEs. We used the *minimize* function from the *scipy.optimize* library with the Nelder–Mead method to minimize the sum of absolute residuals in eqn (2).¹⁴

Fig. 4 compares the calculated and experimental biocrude yields for the data set used to fit and predictions for the model parameters. Table 4 summarizes the statistics for each. The model is able to correlate and predict biocrude yields with a median absolute residual of about 5.5 wt%.

Fig. 5 compares predictions from the new reaction engineering model to predictions from 15 reaction engineering models^{13,27–37} in the literature. Fig. 5a displays violin plots of the distribution of residuals for the new model, three models that explicitly include lignin in biomass, and four models that do not require biomass composition. The new model gives better predictions. Fig. 5b displays violin plots of the distribution of residuals for the new reaction engineering model and eight

models that do not include lignin as part of the biomass. We include data only from HTL of the lignin-void biomass in the testing dataset in Fig. 5b. All the statistical data is provided in the ESI in Tables S2 and S3.†

We also fit the parameters for the reaction networks from Valdez *et al.*,³⁰ Sheehan and Savage,³¹ Obeid *et al.*,³² and Hietala and Savage³³ to the new, larger dataset. The statistics for biocrude fit and predictions are available in Tables S6 and S7.† The results show the new reaction engineering model is superior to the other networks using the same dataset to parameterize all the models.

5 Machine learning model

Machine learning models explain and predict outputs by identifying the connections and patterns between inputs and outputs. These models require user input parameters such as the number of estimators and minimization criteria. To determine the optimal parameters for predictions, we separate the fitting dataset, 90% of the total dataset, into 80% training and 20% testing data subsets. While varying the user input parameters, we optimized the predictions for the 20% testing data subset. We then fit the model to the full 90% fitting dataset and used the optimal parameters to predict the 10% prediction dataset.

Table 4 Statistical analysis for fitting and prediction for the new reaction engineering model

Statistic	Fit	Prediction
Number of data points	1032	112
Med[ε]	-0.0195	0.950
$ \varepsilon $	7.62	8.04
Med[$ \varepsilon $]	5.86	5.53
MAPE	112	77.2
AIC (wt%)	4939.7	—
% < 5	44.5	47.3
% < 10	72.0	67.0

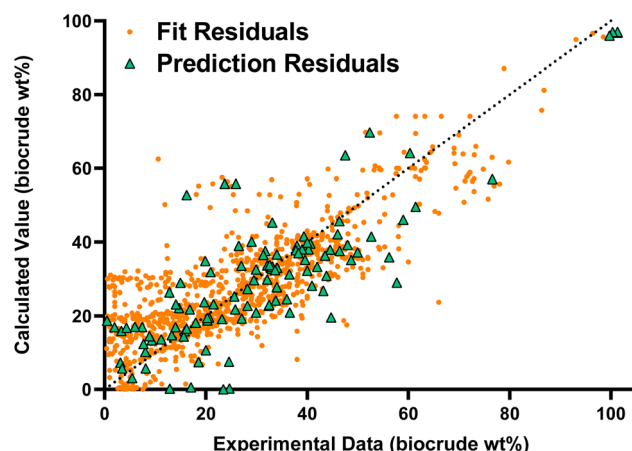


Fig. 4 Parity plot for the new reaction engineering model fit and predictions.



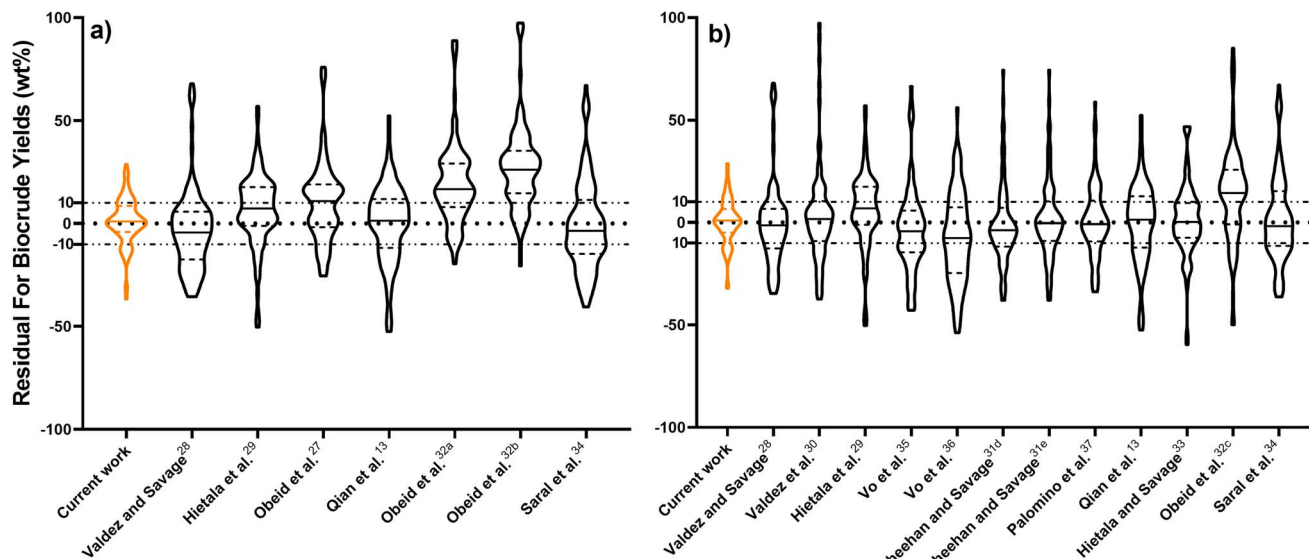


Fig. 5 Predictions from reaction engineering models using a violin plot. The outer curve is the distribution of the residuals, the solid line in the middle is the median residual, and the dashed lines are the upper and lower quartiles: (a) Models suitable for lignin-containing biomass. (b) Models without lignin (88 biocrude yields). ^a The reaction network fitted to HTL of sewage sludge data. ^b The reaction network fitted to HTL of pine wood data. ^c The reaction network fitted to HTL of microalgae data. ^d The reaction network with the interactions. ^e The reaction network including the interactions.

We tested supervised, continuous input and output machine learning models. The model algorithms are from the *sklearn* version 1.4.0 library in *Python* version 3.11.7, 64-bit.³⁸

Of all the machine learning models, the decision tree algorithm provided the highest performance in fitting and predicting of the data. The model is set to a maximum depth of 14, three random states, the minimization criterion set to absolute error, and the rest of the options as default choices. The model results in a 924-leaf tree network. We provide the code on GitHub (https://github.com/pguirguis/Model_Comparison) to print the tree and use it for predictions. The Gaussian Process Algorithm has the optimal statistics (see the ESI†), but its Gaussian structure does not align with the relationship

between the HTL conditions and biocrude yields, resulting in a distinct inability to predict the data accurately. Additionally, the random forest algorithm shows a good fit and the outstanding prediction with 7241 leaves. However, this model is not chosen because its AIC is four times that of the decision tree algorithm. Tables S8–S11† provide statistics for all models that we considered.

Fig. 6 compares the calculated and experimental biocrude yields for the data set used to fit and predictions for the model parameters. Table 5 summarizes the statistics for each. The model predicted biocrude yields to within 4.6 wt% median absolute residual.

6 Comparing the new models

Fig. 7 shows the distribution of the residuals for all three models. Fig. 7a is the distribution for fitting each model to the literature dataset and Fig. 7b is the distribution for predictions.

Table 5 Statistical analysis for fitting and prediction for the new decision tree model with 924 parameters

Statistic	Fit	Prediction
Number of data points	1032	112
Med[ε]	0.00	1.08
$\overline{ \varepsilon }$	0.230	6.64
Med[$ \varepsilon $]	0.00	4.60
MAPE	1.36	43.5
AIC (wt%)	2049.4	—
% < 5	98.5	52.7
% < 10	99.8	80.4

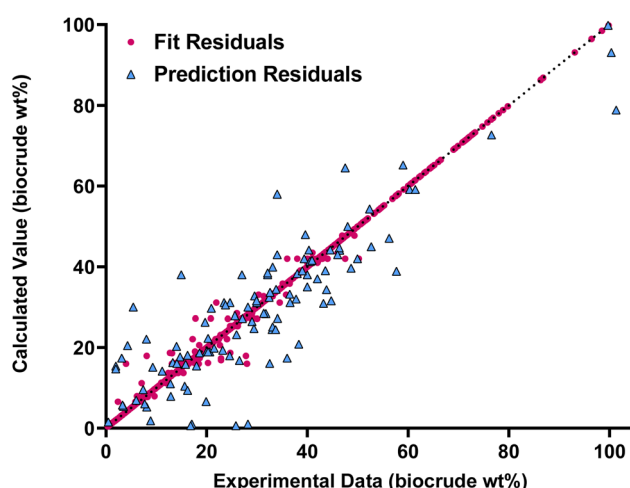


Fig. 6 Parity plot for the new decision tree model fit and predictions.



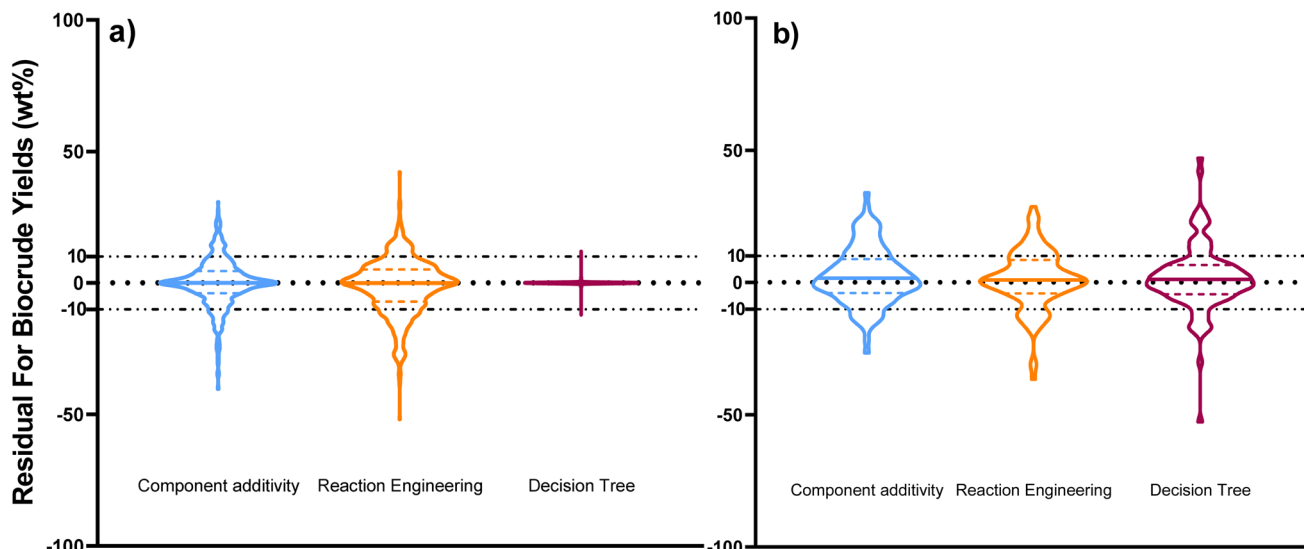


Fig. 7 Residuals from calculating biocrude yields with each new model using a violin plot. The outer curve is the distribution of the residuals, the solid line in the middle is the median residual, and the dashed lines are the upper and lower quartiles: (a) Model fitting, (b) model predictions.

The decision tree model fits the data the best. It also has the largest number of parameters, with 924 leaves. The model uses a set of “decisions” to reach its predictions, and 868 out of the 924 leaves contain a single data point. The component additivity model, with 150 parameters, has lower error than the reaction engineering model, which has 56 parameters. The component additivity model uses additional parameters to correlate and predict the effects of biomass loading (wt%). For predictions, the decision tree model had the smallest median absolute error of 4.6 wt%, but it also gives the widest distribution of residuals. The component additivity model has the smallest distribution of residuals and its median absolute error was 6.33 wt%. The reaction engineering model performed similarly and has a median absolute residual of 5.53 wt%.

7 Predictions for new biomass feedstocks

In this section, we use the new models to estimate the highest biocrude yields available from HTL of different biomass feedstocks, along with the corresponding HTL conditions. The feedstocks and their compositions are listed in Table 6. Three

feedstocks have a high carbohydrate content. One is high in cellulose (hemp fiber), one is high in starch (macaroni noodles), and one is high in other carbohydrates (watermelon rinds). We selected one feedstock with high lipid content, which also has the highest protein content (mechanically deboned chicken meat), and one with high lignin content (apple pomace). In nature, biomass with high hemicellulose or lignin content typically also contains a significant amount of cellulose. The apricot kernel press cake contains all four components in relatively balanced proportions. Cheese sauce contains nearly equal amounts of starch and protein, along with lipids. Finally, we considered the mixture of cheese sauce and macaroni, as described in Wang *et al.*⁴⁴

Table 7 presents the conditions for HTL predicted by each model to give the highest possible biocrude yield.

Since the machine learning model is made of discrete choices, we use a grid of 1000 steps for time between 0–3 h, loading mass between 0–40 (g solids/g water)%), and temperature between 0–650 °C to find the maximum biocrude yield. The decision tree model uses discrete “decisions” or “leaves” to fit the data, which aligns the predictions closely with the correlating data. The large number of “N/A” entries in Table 7 for the decision tree model however, indicates the model has difficulty

Table 6 New biomass feedstocks and their composition

Ref.	Feedstock	C_t	Un	Ce	He	St	P_t	F_t	L_t	Ash
Jawaaid and Abdul Khalil ³⁹	Hemp fiber	92.3	0	74.4	17.9	0	0	1.30	3.70	N/A
Arivuchudar ⁴⁰	Watermelon rinds	62.8	62.8	0	0	0	12.5	2.74	0	14.7
Selmane <i>et al.</i> ⁴¹	Mechanically deboned chicken meat	0	0	0	0	0	52.7	42.5	0	N/A
Vendruscolo <i>et al.</i> ⁴²	Apple pomace	59.8	59.8	0	0	0	5.90	0	38.2	3.50
Sharma <i>et al.</i> ⁴³	Apricot kernel press cake	27.5	27.5	0	0	0	34.3	9.70	10.8	N/A
Wang <i>et al.</i> ⁴⁴	Cooked macaroni noodles	83.9	0	0	0	83.9	14.0	1.35	0	0.800
	Cheese sauce	42.9	0	0	0	42.9	41.5	12.6	0	3.03
	Macaroni and cheese	70.9	0	0	0	70.9	13.5	14.1	0	1.51



Table 7 Model predictions for highest biocrude yields and HTL conditions for new feedstocks^a

Ref.	Feedstock	Component additivity model			Reaction engineering model			Decision tree model						
		Biocrude (wt%)	Solids (g g ⁻¹ %)	In(SI)	Biocrude (wt%)	Time (min)	Temp. (°C)	*b (min ⁻¹)	In(SI)	Biocrude (wt%)	Solids (g g ⁻¹ %)	Time (min)	Temp. (°C)	In(SI)
Jawaid and Abdul Khalil ³⁹	Hemp fiber	28.2	1.87	1.23	31.5	0.770	556	Iso	1.96	22.1	N/A	N/A	480	N/A
Arivuchudar ⁴⁰	Watermelon rinds	22.5	10.7	1.76	31.8	0.656	560	Iso	1.86	17.0	29.0	15.5	328	1.02
Selmane <i>et al.</i> ⁴¹	Mechanically deboned chicken meat	63.9	12.5	6.05	54.1	2.84	388	Iso	0.212	66.0	13.4	1.03	575	2.52
Vendruscolo <i>et al.</i> ⁴²	Apple pomace	22.8	17.7	1.84	20.3	1.52	328	1.99	2.67	23.1	N/A	N/A	475	N/A
Sharma <i>et al.</i> ⁴³	Apricot kernel press cake	36.7	18.4	1.60	47.4	1.37	479	Iso	1.30	66.0	13.4	1.03	575	2.52
Wang <i>et al.</i> ⁴⁴	Cooked macaroni noodles	39.4	N/A	1.71	36.5	0.322	591	Iso	1.55	32.0	N/A	2.83	31.3	-1.73
	Cheese sauce	49.1	0.734	1.75	48.7	1.39	467	Iso	1.09	66.0	13.4	1.03	575	2.52
	Macaroni and cheese	51.1	0.185	1.69	41.9	0.475	542	Iso	1.26	66.0	13.4	1.03	575	2.52

^a *b is the constant for the heating profile in eqn (8). N/A means the model did not move that value from its initial state, Iso means isothermal.

with feedstocks that do not closely match those used to determine the parameters. Additionally, predictions for four out of the eight feedstocks give the same yield and HTL conditions despite the feedstocks having very different compositions. This is a disadvantage of using a discrete model such as the decision tree. When examining predictions for a larger dataset of 39 new biomass feedstocks, we find only 11 unique optimal conditions for the decision tree machine learning model.

The three models agree that HTL of the biomasses with large fractions of carbohydrates have a lower maximum biocrude yield than the other feedstocks. Additionally, HTL of mechanically deboned chicken meat, high in fat and proteins, gives the highest biocrude yield for each model. Finally, all the models predict a higher biocrude yield for HTL of the macaroni and cheese together rather than separately. The predicted increase in biocrude yield is 8.75 wt%, 1.56 wt%, and 23.25 wt% for component additivity model, reaction engineering model, and decision tree model, respectively.

The models show large disagreement for HTL conditions for a few feedstocks. For mechanically deboned chicken meat and cheese sauce, the reaction engineering model predicts milder conditions than does the component additivity model. The models also disagree as to the reaction severity needed to liquefy the cooked macaroni noodles, cheese sauce, and macaroni and cheese. The decision tree model has the highest severity, the component additivity model has a medium severity, and the reaction engineering model gives the mildest conditions.

The apricot kernel press cake is the only new feedstock considered here that contains at least 10% each of carbohydrates, proteins, lipids, and lignin. Containing all these components in appreciable amounts makes this material an interesting biomass feedstock for testing the models. The three models disagree on the severity of the HTL conditions and the highest biocrude yield that can be obtained. Fig. 8 examines HTL of this feedstock in greater detail. The figure shows the biocrude yields calculated from each model over a wide range of HTL temperatures and times. The colors correspond to the biocrude yields. Fig. 8a shows the component additivity model predicts biocrude yields up to about 35 wt% follow a narrow band on the plot. Fig. 8b shows the reaction engineering model predicts biocrude yields of about 50 wt% at short times over a range of supercritical temperatures. Fig. 8c shows discrete “decision” boxes and there are no smooth transitions between the boxes.

8 Closing perspective

This work provides new models for predicting yields of biocrude from HTL of biomass. These models predicted literature data better than did previous models. The highest median absolute residual for predicting the biocrude yields was 6.3 wt%. The decision tree model fit and predicted the dataset significantly better than the new component additivity and reaction engineering models. The component additivity model is statistically better at fitting the dataset than the reaction engineering model and the reaction engineering model is better at predicting the

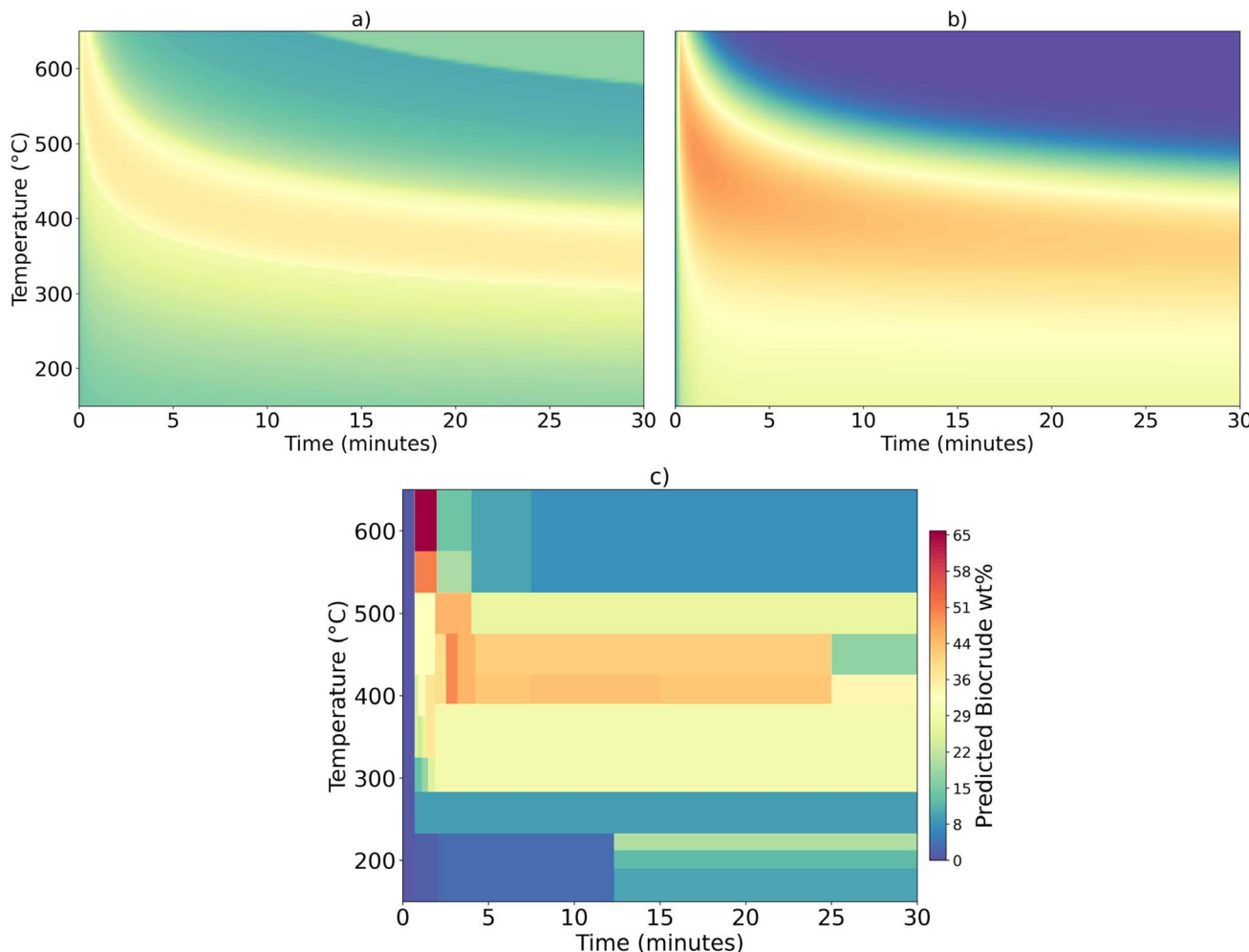


Fig. 8 Biocrude yield predicted for isothermal HTL of apricot kernel press cake. (a) Component additivity model at 18.43 wt% loading (b) reaction engineering model (c) decision tree model at 13.45 wt% loading.

dataset than the component additivity model. When seeking the optimal HTL conditions for new feedstocks, the discrete “leaves” from the decision tree model limits the model predictions.

The models are general in that they can be applied to nearly any biomass feedstock and over a very wide range of potential HTL reaction conditions. As such, the models can be used to guide experimental work. They can also be employed in techno-economic analyses and life cycle assessments to investigate the influence of biomass composition and HTL processing conditions on the profitability and environmental impacts of HTL conversion.

The present modeling work accepted all literature data as being of equal value. We believe even better models could be developed if there were a carefully curated set of experimental data for HTL. Ideally, the same biomass feedstocks and same sets of reaction conditions would be examined in multiple labs and the resulting data then combined and assessed. Such a harmonized data set, which would include experimental uncertainties, would be a tremendous asset in improving the general models for HTL of biomass.

The three different approaches for modeling used herein have comparative advantages and disadvantages. Component additivity models are conceptually simple and provide a connection to the physical system. They can be expanded as needed to account for statistically meaningful interactions between components. Decision tree models can do a great job of fitting data, but the predictive ability is not as good as the correlating ability (at least in the present study). Also, the decision tree has no connection to the physical situation and it is a discrete model whereas process variables are continuous. Reaction engineering models can provide predictions for all components in the reacting system – not just biocrude. That is, the model can predict (or correlate) the yields of aqueous-phase products and gaseous products as well. Moreover, a reaction engineering model can be made even more “molecular” by adopting reaction pathways that are more closely connected to the overall chemical conversions taking place (e.g., protein decomposing to peptides that decompose to amino acids that decomposes further by deamination or decarboxylation).

Each model has limitations. Using the severity index in the component additivity model ignores the individual effects of



time and temperature. As a result, the conditions obtained when optimizing feedstocks include a set of temperature and time for the optimal severity index. The reaction engineering model is the only model that does not include any dependence of HTL outcomes on the wt% loading in the reactor, though this is known to have an effect for some biomass components. The decision tree model predicts biocrude yields based on given feedstock composition and HTL conditions. Its accuracy depends on the similarity between the input data and the training set. When inputs closely match the training data, predictions are reliable. However, if the training set lacks similar feedstock compositions and HTL conditions, the model may produce inaccurate predictions. With a large training dataset and numerous input parameters, identifying the specific feedstock compositions and HTL conditions needed to prevent inaccurate predictions becomes challenging. This limitation is evident when optimizing HTL conditions for the feedstocks tested in this study.

Data availability

The three models and the data associated with them are available on GitHub (https://github.com/pguirguis/Model_Comparison).

Author contributions

Peter M. Guirguis: conceptualization, data curation, formal analysis, validation, visualization, writing – original draft, writing – review & editing, and Phillip E. Savage: conceptualization, funding acquisition, methodology, project administration, supervision, writing – review & editing.

Conflicts of interest

There are no conflicts to declare.

Acknowledgements

This work was supported with funds from the Walter L. Robb Family Chair in Chemical Engineering at Penn State.

Notes and references

- 1 M. Shahabuddin, N. Kazantzis, A. R. Teixeira and M. T. Timko, *Energy Convers. Manage.*, 2024, **24**, 100756.
- 2 Y. Jiang, S. B. Jones, Y. Zhu, L. Snowden-Swan, A. J. Schmidt, J. M. Billing and D. Anderson, *Algal Res.*, 2019, **39**, 101450.
- 3 P. H. Chen and J. C. Quinn, *Appl. Energy*, 2021, **289**, 116613.
- 4 M. Pearce, M. Shemfe and C. Sansom, *Appl. Energy*, 2016, **166**, 19–26.
- 5 L. Ou, R. Thilakaratne, R. C. Brown and M. M. Wright, *Biomass Bioenergy*, 2015, **72**, 45–54.
- 6 P. Ranganathan and S. Savithri, *Bioresour. Technol.*, 2019, **284**, 256–265.
- 7 Y. Zhu, M. J. Biddy, S. B. Jones, D. C. Elliott and A. J. Schmidt, *Appl. Energy*, 2014, **129**, 384–394.
- 8 P. M. Guirguis, M. S. Seshasayee, B. Motavaf and P. E. Savage, *RSC Sustainability*, 2024, **2**, 736–756.
- 9 G. Teri, L. Luo and P. E. Savage, *Energy Fuels*, 2014, **28**, 7501–7509.
- 10 J. Wagner, R. Bransgrove, T. A. Beacham, M. J. Allen, K. Meixner, B. Drosig, V. P. Ting and C. J. Chuck, *Bioresour. Technol.*, 2016, **207**, 166–174.
- 11 R. Shakya, S. Adhikari, R. Mahadevan, S. R. Shanmugam, H. Nam, E. B. Hassan and T. A. Dempster, *Bioresour. Technol.*, 2017, **243**, 1112–1120.
- 12 S. Mahadevan Subramanya and P. E. Savage, *ACS Sustain. Chem. Eng.*, 2021, **9**, 13874–13882.
- 13 L. Qian, S. Wang and P. E. Savage, *Appl. Energy*, 2020, **260**, 114312.
- 14 P. Virtanen, R. Gommers, T. E. Oliphant, M. Haberland, T. Reddy, D. Cournapeau, E. Burovski, P. Peterson, W. Weckesser, J. Bright, S. J. van der Walt, M. Brett, J. Wilson, K. J. Millman, N. Mayorov, A. R. J. Nelson, E. Jones, R. Kern, E. Larson, C. J. Carey, Å. Polat, Y. Feng, E. W. Moore, J. VanderPlas, D. Laxalde, J. Perktold, R. Cimrman, I. Henriksen, E. A. Quintero, C. R. Harris, A. M. Archibald, A. H. Ribeiro, F. Pedregosa, P. van Mulbregt, A. Vijaykumar, A. P. Bardelli, A. Rothberg, A. Hilboll, A. Kloeckner, A. Scopatz, A. Lee, A. Rokem, C. N. Woods, C. Fulton, C. Masson, C. Häggström, C. Fitzgerald, D. A. Nicholson, D. R. Hagen, D. V. Pasechnik, E. Olivetti, E. Martin, E. Wieser, F. Silva, F. Lenders, F. Wilhelm, G. Young, G. A. Price, G.-L. Ingold, G. E. Allen, G. R. Lee, H. Audren, I. Probst, J. P. Dietrich, J. Silterra, J. T. Webber, J. Slavić, J. Nothman, J. Buchner, J. Kulick, J. L. Schönberger, J. V. de Miranda Cardoso, J. Reimer, J. Harrington, J. L. C. Rodríguez, J. Nunez-Iglesias, J. Kuczynski, K. Tritz, M. Thoma, M. Newville, M. Kümmerer, M. Bolingbroke, M. Tartre, M. Pak, N. J. Smith, N. Nowaczyk, N. Shebanov, O. Pavlyk, P. A. Brodtkorb, P. Lee, R. T. McGibbon, R. Feldbauer, S. Lewis, S. Tygier, S. Sievert, S. Vigna, S. Peterson, S. More, T. Pudlik, T. Oshima, T. J. Pingel, T. P. Robitaille, T. Spura, T. R. Jones, T. Cera, T. Leslie, T. Zito, T. Krauss, U. Upadhyay, Y. O. Halchenko and Y. Vázquez-Baeza, *Nat. Methods*, 2020, **17**, 261–272.
- 15 A. Gollakota and P. E. Savage, *Energy Fuels*, 2019, **33**, 11328–11338.
- 16 M. Déniel, G. Haarlemmer, A. Roubaud, E. Weiss-Hortal and J. Fages, *Waste Biomass Valorization*, 2017, **8**, 2087–2107.
- 17 J. Yang, Q. S. He, H. Niu, K. Corscadden and T. Astatkine, *Appl. Energy*, 2018, **228**, 1618–1628.
- 18 J. Lu, Z. Liu, Y. Zhang and P. E. Savage, *ACS Sustain. Chem. Eng.*, 2018, **6**, 14501–14509.
- 19 J. Yang, Q. S. He, K. Corscadden, H. Niu, J. Lin and T. Astatkine, *Appl. Energy*, 2019, **233–234**, 906–915.
- 20 P. Biller and A. B. Ross, *Bioresour. Technol.*, 2011, **102**, 215–225.
- 21 S. Leow, J. R. Witter, D. R. Vardon, B. K. Sharma, J. S. Guest and T. J. Strathmann, *Green Chem.*, 2015, **17**, 3584–3599.
- 22 Y. Li, S. Leow, A. C. Fedders, B. K. Sharma, J. S. Guest and T. J. Strathmann, *Green Chem.*, 2017, **19**, 1163–1174.



23 D. C. Hietala, C. K. Koss, A. Narwani, A. R. Lashaway, C. M. Godwin, B. J. Cardinale and P. E. Savage, *Algal Res.*, 2017, **26**, 203–214.

24 L. Sheng, X. Wang and X. Yang, *Bioresour. Technol.*, 2018, **247**, 14–20.

25 A. Aierzhati, M. J. Stablein, N. E. Wu, C.-T. Kuo, B. Si, X. Kang and Y. Zhang, *Bioresour. Technol.*, 2019, **284**, 139–147.

26 R. Obeid, D. M. Lewis, N. Smith, T. Hall and P. van Eyk, *Chem. Eng. J.*, 2020, **389**, 124397.

27 R. Obeid, D. M. Lewis, N. Smith, T. Hall and P. van Eyk, *Energy Fuels*, 2020, **34**, 419–429.

28 P. J. Valdez and P. E. Savage, *Algal Res.*, 2013, **2**, 416–425.

29 D. C. Hietala, J. L. Faeth and P. E. Savage, *Bioresour. Technol.*, 2016, **214**, 102–111.

30 P. J. Valdez, V. J. Tocco and P. E. Savage, *Bioresour. Technol.*, 2014, **163**, 123–127.

31 J. D. Sheehan and P. E. Savage, *Bioresour. Technol.*, 2017, **239**, 144–150.

32 R. Obeid, N. Smith, D. M. Lewis, T. Hall and P. van Eyk, *Chem. Eng. J.*, 2022, **428**, 131228.

33 D. C. Hietala and P. E. Savage, *Chem. Eng. J.*, 2021, **407**, 127007.

34 J. S. Saral, D. G. C. V. Reddy and P. Ranganathan, *Biomass Convers. Biorefin.*, 2022, **1**, 1–9.

35 T. K. Vo, O. K. Lee, E. Y. Lee, C. H. Kim, J.-W. Seo, J. Kim and S.-S. Kim, *Chem. Eng. J.*, 2016, **306**, 763–771.

36 T. K. Vo, S.-S. Kim, H. V. Ly, E. Y. Lee, C.-G. Lee and J. Kim, *Bioresour. Technol.*, 2017, **241**, 610–619.

37 A. Palomino, L. C. Montenegro-Ruiz and R. D. Godoy-Silva, *Algal Res.*, 2019, **44**, 101669.

38 F. Pedregosa, G. Varoquaux, A. Gramfort, V. Michel, B. Thirion, O. Grisel, M. Blondel, P. Prettenhofer, R. Weiss, V. Dubourg, J. Vanderplas, A. Passos, D. Cournapeau, M. Brucher, M. Perrot and E. Duchesnay, *J. Mach. Learn. Res.*, 2011, **12**, 2825–2830.

39 M. Jawaid and H. Abdul Khalil, *Carbohydr. Polym.*, 2011, **86**, 1–18.

40 R. Arivuchadar, *Biosci., Biotechnol. Res. Asia*, 2023, **20**, 263–269.

41 D. Selmane, V. Christophe and D. Gholamreza, *Meat Sci.*, 2008, **79**, 640–647.

42 F. Vendruscolo, P. M. Albuquerque, F. Streit, E. Esposito and J. L. Ninow, *Crit. Rev. Biotechnol.*, 2008, **28**, 1–12.

43 P. C. Sharma, B. M. K. S. Tilakratne and A. Gupta, *J. Food Sci. Technol.*, 2010, **47**, 682–685.

44 Y. Wang, T. D. Wig, J. Tang and L. M. Hallberg, *J. Food Eng.*, 2003, **57**, 257–268.

